ROYAL SOCIETY
OF CHEMISTRY

COMMUNICATION

Check for updates

Aggregation-induced emission luminogen with excellent triplet–triplet upconversion efficiency for highly efficient non-doped blue organic light-emitting diodes†

Pengbo Han,[a] Chengwei Lin, [ID][a] Kaojin Wang,[a] Yanping Qiu,[a] Haozhong Wu,[a] Anjun Qin, [ID] *[a] Dongge Ma [ID] *[a] and Ben Zhong Tang [ID] *[ab]

By combining aggregation-induced emission (AIE) effect and a triplet–triplet upconversion (TTU) process, a blue emitter with excellent photoluminescence quantum efficiency and high upconversion efficiency in the film state is developed, from which a highly efficient non-doped blue TTU organic light-emitting diode (TTU-OLED) was realized.

Organic light-emitting diodes (OLEDs) have been widely used in the field of full-color, flat-panel displays and white lighting.[1] In OLEDs, injected electrons and holes recombine to form 25% singlet excitons and 75% triplet excitons.[2] Therefore, the most effective method of enhancing the efficiency of OLEDs involve contributions of triplet excitons. Phosphorescent OLEDs (Ph-OLEDs) containing transition metal complexes can achieve 100% internal quantum efficiency (IQE) through the strong spin–orbit coupling effect of heavy atoms.[3] Alternatively, the lowest triplet (T_1) excitons can be up-converted to singlet (S_1) ones through a reverse intersystem crossing (RISC) process to realize thermally activated delayed fluorescence (TADF),[4] leading to a nearly 100% IQE.[5] Although blue Ph- and TADF-OLEDs can harvest triplet excitons efficiently, their operation lifetime and efficiency roll-off at high voltages are still a hindrance due to their long exciton lifetime and high triplet energy levels.[6] Meanwhile, low T_1 excitons can be theoretically converted into the high S_1 ones through a triplet fusion (TF) process to make use of triplet excitons.[7] Triplet–triplet upconversion (TTU)

[a] State Key Laboratory of Luminescent Materials and Devices, Guangdong Provincial Key Laboratory of Luminescence from Molecular Aggregates, Center for Aggregation-Induced Emission, South China University of Technology, Guangzhou, Guangdong 510640, China. E-mail: msdgma@scut.edu.cn, msqinaj@scut.edu.cn

[b] Shenzhen Institute of Molecular Aggregate Science and Engineering, School of Science and Engineering, The Chinese University of Hong Kong, Shenzhen, 2001 Longxiang Boulevard, Longgang District, Shenzhen City, Guangdong 518172, China. E-mail: tangbenz@cuhk.edu.cn

New concepts

Triplet–triplet upconversion (TTU), where two low-energy triplet excitons are converted to one higher energy singlet exciton, is an excellent approach to break through the theoretical limit of the pure fluorescent organic light-emitting diodes (OLEDs) by 5%. To date, however, reported emitters with high emission efficiency and excellent TTU efficiency in the film state are rare. Herein, for the first time, we report an efficient non-doped blue OLED using anthracene-based AIEgens with a TTU process through spin–orbit coupling. The as-developed AIEgens exhibit high emission efficiency and an excellent triplet upconversion efficiency close to 50% in the film states, ultimately leading to the efficient blue TTU-OLED with an external quantum efficiency of 8.1%. The excellent device performance suggests that the molecular design principle proposed herein is powerful for the development of TTU-OLEDs with high performance and low roll-off efficiency.

OLEDs can not only achieve a high IQE, but also possess long operation lifetimes compared to those of blue TADF and Ph-OLEDs.[8] Therefore, it is highly desirable to develop efficient blue TTU-OLEDs.

As shown in Fig. 1A, two triplet fusion generates an intermediate state ($T_1 + T_1$), whose spin–spin coupling leads to the formation of 1/9 singlets $^1(TT)$, 1/3 triplets $^3(TT)$, and 5/9 quintets $^5(TT)$.[9] The $^1(TT)$ and $^3(TT)$ can form S_1 and T_1 with a molecular ground state (S_0), respectively. Conversely, $^5(TT)$ could be up-converted to the $T_1 + T_1$ intermediate state, because its energy is lower than that of the quintet (intramolecular) excited state (Q_1).[8c] Therefore, T_1 can form S_0 *via* a repeated TF process with an upconversion efficiency (η_{TTU}) of close to 20%.[9a] When the energy level of T_2 is higher than that of $2T_1$, $^3(TT)$ can be expected to return directly to $2T_1$, and the η_{TTU} can be also raised to 50%.[10] However, the high TF efficiency is only limited to some special materials, such as anthracene derivatives and rubrene, because of the strict energetic requirements.[8a,11] Alternatively, the transition from $^3(TT)$ to S_1 has been suggested to break through the limit of η_{TTU}.[12] Although it is a promising pathway to improve η_{TTU}, blue OLEDs with high-performance based on these transitions are

Fig. 1 (A) Energy-level diagram illustrating the mechanisms of triplet–triplet upconversion (TTU) and triplet–triplet annihilation (TTA). ^{1}(TT), ^{3}(TT), and ^{5}(TT) are the singlet, triplet, and quintet intermediate states. S_1, T_1, and S_0 are singlet excitons, triplet excitons, and ground states. S_n and T_n are higher singlet and triplet states. (B) Chemical structures of the anthracene derivatives. (C) Design principle of the blue emitters.

rare because of the absence of effective molecular design strategies.

9,10-Diphenylanthracene (DPA), a polycyclic aromatic hydrocarbon (PAH) compound with a low triplet energy level and good stability, is typically used as an emitter for the construction of blue TTU OLEDs.[13] In principle, TTU is a bimolecular process and needs a high enough triplet exciton concentration to improve the TF efficiency. However, DPA is usually doped into appropriate host materials due to its aggregation-caused quenching (ACQ) effects.[14] As a result, it is difficult for the doped devices to achieve high-performance blue OLEDs by controlling the TF process. More importantly, preparation of the doped devices is complicated. Therefore, developing PAH compounds with intense emission in the film state is beneficial for the construction of high-performance non-doped blue TTU-OLEDs.

Exactly opposite to the ACQ effect, luminogens with aggregation-induced emission characteristics (AIEgens) can exhibit intense emission in their film states.[15] Thus, they are ideal candidates to combine PAH compounds with TTU features to solve the above problems. According to our reported design strategy, new AIEgens, decorated ACQ molecules with a triphenylamine (TPA) moiety, have also been achieved.[16] In addition, Konishi *et al.* illustrated that the frontier orbitals of diarylamine and anthracene interpenetrated when the planar donor was distorted,[17] meanwhile, a transition between molecular orbitals with relative orthogonal directions might also promote the conversion process from ^{3}(TT) to S_1.[12]

Herein, the compounds TPA-An-Ph and TPA-An-mPhCz, in which the twisted donating groups of triphenylamine (TPA) was attached on anthracene (An) cores together with the *meta*-positions substituted planar group of the carbazole (Cz) moiety

in the latter, were designed and synthesized (Fig. 1B). The carbazole group can facilitate the hole transport of devices, which in turn improves the device performance.[18] In addition, it was demonstrated that high-efficiency emission in the solid state can be achieved using the *meta*-substituted strategy.[19] Thanks to their AIE features, TPA-An-Ph and TPA-Ph-mPhCz show high photoluminescence quantum efficiency yields (PLQYs, Φ_F) in their film states. The non-doped OLEDs using these AIEgens as emitting layers (EMLs) show blue emission and exhibit low efficiency roll off. The TPA-An-Ph-based OLED gives a maximum forward-viewing external quantum efficiency (EQE) of 4.51%. Notably, the TPA-An-mPhCz-based OLED achieves a maximum EQE of 8.1%. The transient electroluminescence (EL) spectra and theoretical calculations suggest that this could be ascribed to the effective TTU conversion process from ^{3}(TT) to S_n of TPA-An-mPhCz. This strategy might provide an instructive way to achieve highly efficient commercialized blue OLEDs using the construction of AIEgens with an effective TTU process (Fig. 1C).

The synthetic routes to TPA-An-Ph and TPA-An-mPhCz are shown in Scheme S1 (ESI†). They could be facilely synthesized in 80% yields using the Suzuki coupling reaction. The structures of TPA-An-Ph and TPA-An-mPhCz were fully characterized using ^{1}H and ^{13}C NMR and high resolution mass (HRMS) spectroscopies. For comparison, the commercialized DPA was used to explore the rationality of the design. DPA, TPA-An-Ph and TPA-An-mPhCz are soluble in commonly used organic solvents, such as dichloromethane (DCM) and tetrahydrofuran (THF), but insoluble in water.

After confirming their structures, the photophysical properties of DPA, TPA-An-Ph and TPA-An-mPhCz were studied. Fig. 2A shows their ultraviolet-visible (UV-vis) absorption spectra in THF solutions. The absorption band at 360–400 nm could readily be assigned to the π–π* transition of the anthracene core.[20] The PL spectra of DPA, TPA-An-Ph and TPA-An-mPhCz in THF solutions exhibit deep blue and blue emissions with peaks ranging from 409 to 476 nm upon photoexcitation (Fig. S1, ESI†). In comparison with DPA in a THF solution, the emission peaks of TPA-An-Ph and TPA-An-mPhCz were considerably red-shifted because of the enlongation of the conjugation. Meanwhile, featureless PL spectra were obtained for TPA-An-Ph and TPA-An-mPhCz in THF solutions, implying that each emission originates from the charge transfer (CT) state. The PL spectra of the vacuum-deposited neat films of DPA, TPA-An-Ph, and TPA-An-mPhCz show deep blue and blue emission with peaks at 442, 460 and 470 nm, respectively (Fig. 2B). The Φ_F value of DPA in a THF solution was 68.1%, but reduced to 59.3% in the vacuum-deposited neat film. Notably, the Φ_F values of TPA-An-Ph and TPA-An-mPhCz in THF solutions were measured to be 30.0 and 57.8%, and further enhanced to 40.1% and 65.1% in their vacuum-deposited neat films, respectively. These results suggest that TPA-An-Ph and TPA-An-mPhCz exhibit the aggregation-enhanced emission (AEE) feature.

To further explore the AEE feature of TPA-An-Ph and TPA-An-mPhCz, their PL behavior was explored in THF/water mixtures
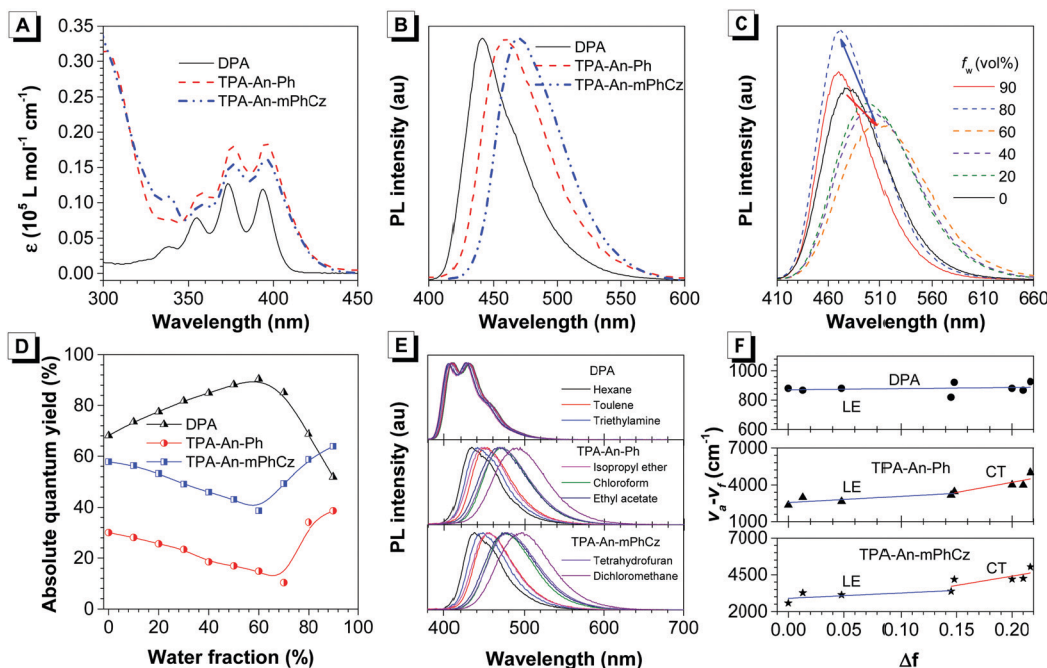
Fig. 2 (A) UV-Vis (THF solution) and (B) photoluminescence (PL, film state) spectra of DPA, TPA–An–Ph, and TPA–An–mPhCz. (C) PL spectra of TPA–An–mPhCz in THF/water mixtures with different water fractions (f_w); λ_{ex}: 360 nm; concentration: 10 μM. (D) Absolute photoluminescence quantum yield of DPA, TPA–An–Ph, and TPA–An–mPhCz *versus* water fractions in THF/water mixtures. (E) Effects of solvent on the fluorescence spectra of the anthracene derivatives. (F) Stokes shifts of the anthracene derivatives as a function of the orientation polarizability. The solid lines are the fitting results using the Lippert–Mataga equation.

with different water fractions (f_w). As shown in Fig. 2C and Fig. S2 (ESI†), the emission peaks slowly red-shifted along with the decrease in PL intensity when f_w was gradually increased, which is attributed to the process of twisted intramolecular charge transfer (TICT).[21] However, when the f_w was further increased, their PL gradually intensified along with the blue-shifted emission peak owing to the formation of aggregates and activation of the restriction of intramolecular motion (RIM).[22] In contrast with TPA–An–Ph and TPA–An–mPhCz, the Φ_F values of DPA in THF/water mixtures with different f_w show a completely opposite trend (Fig. 2D), which further demonstrated the effectiveness of our design strategy.

To concretely analyze the excited states of DPA, TPA–An–Ph and TPA–An–mPhCz, their PL spectra were investigated in different solvents (Fig. 2E). According to the Lippert–Mataga model,[23] the dipole moments of their excited state can be acquired using the slope of the Stokes shift (v_a-v_f) as a function of the orientation polarizability (f) as shown in Tables S1–S3 (ESI†). The fitting results are shown in Fig. 2F. The derived dipole moment (μ_e) of the excited state of DPA is 0.69 D, indicating that its excited state could be assigned to the localized excited (LE) state. While, TPA–An–Ph and TPA–An–mPhCz exhibit two independent slopes: smaller μ_e values of 7.27 and 9.02 D in low polarity solvents and larger μ_e values of 12.93 and 14.95 D in highly polar solvents, respectively. These results suggest that their excited states are assigned to the LE and CT states, respectively. Furthermore, their PL spectra in the film state were measured at 77 K (Fig. S3, ESI†), and the peaks

of DPA, TPA–An–Ph and TPA–An–mPhCz were recorded to be 424 nm (2.92 eV), 454 nm (2.73 eV), and 467 nm (2.66 eV), respectively. The PL spectra of TPA–An–Ph and TPA–An–mPhCz in the film state are close to those in the polar solvents rather than those in nonpolar solvents. Therefore, the S_1 states of the TPA–An–Ph and TPA–An–mPhCz films could be assigned to a ^{1}CT mixing weak ^{1}LE state. Moreover, the PL decay curves of DPA, TPA–An–Ph and TPA–An–mPhCz were plotted in Fig. S4 (ESI†). Their lifetime shows a single-exponential decay process in the THF solutions and solid films, suggesting that they emit fluorescence.

To have a deeper understanding of the structure–property relationship, a single crystal of TPA–An–mPhCz (CCDC 2042010†) was obtained *via* a solvent evaporation method and analyzed using X-ray diffraction crystallography. As shown in Fig. 3A, TPA–An–mPhCz possesses a highly twisted L-shape molecular configuration with large dihedral angles distributed between 61° and 81°. Moreover, strong multiple intermolecular C–H⋯π hydrogen bonds with short distances of 2.702–3.721 Å are found between the molecules (Fig. 3B). Notably, no close π–π stacking interaction was found in Fig. 3C and D. These factors can effectively rigidify the molecular conformation and reduce non-radiative energy dissipation in the aggregate state, resulting in an AEE effect.[24]

Besides their high Φ_F values in the film states, TPA–An–Ph and TPA–An–mPhCz are thermally stable according to the differential scanning calorimetry (DSC) and thermogravimetric analysis (TGA) measurements. As depicted in Fig. S5 and

Fig. 3 (A) Crystal structure and (B) packing pattern of TPA-An-mPhCz single crystals; (C) front view and (D) side view of the detailed molecular stacking within the red dotted line.

Table S4 (ESI†), the decomposition temperatures (T_d, 5% weight loss) of TPA-An-Ph and TPA-An-mPhCz are 362 and 411 °C, respectively, and no glass transition temperatures (T_g) were found in the measurement region. These results suggest that they are suitable for the preparation of vapor deposition devices. In addition, the electrochemical properties of TPA-An-Ph and TPA-An-mPhCz were measured using cyclic voltammetry (CV). As shown in Fig. S6 (ESI†), the highest occupied molecular orbital (HOMO) energy levels of TPA-An-Ph and TPA-An-mPhCz are deduced to be −5.20 and −5.22 eV, and their lowest unoccupied molecular orbital (LUMO) energy levels are −2.51 and −2.52 eV, respectively, which will facilitate the device configuration optimization.

Thanks to the excellent thermal stability and the high emission efficiency in the aggregate/film states, the non-doped devices B1 and B2 were constructed using TPA-An-Ph and TPA-An-mPhCz as EMLs, respectively, with a device configuration of ITO/HAT-CN (5 nm)/TAPC (60 nm)/TCTA (5 nm)/EMLs (20 nm)/TmPyPB (40 nm)/LiF (1 nm)/Al (Fig. 4A), where ITO, 1,4,5,8,9,11-hexaazatriphenylene-hexacarbonitrile (HAT-CN), 1-bis[4-[N,N-di(4-tolyl)amino]-phenyl]-cyclo-hexane (TAPC), 4,4′,4″-tri(N-carbazolyl)-triphenylamine (TCTA), and 1,3,5-tri[(3-pyridyl)-phen-3-yl]benzene (TmPyPB) act as the anode, hole injector, hole-transporter, exciton-blocking layer, and electron-transporting layer, respectively. These non-doped OLEDs emit blue light and exhibit excellent device performance at low operation voltages (Fig. 4B). It is worth noting that the EL spectra remain stable when the voltage increased from 3 to 8 V, confirming their good color stability (Fig. 4C and Fig. S7, ESI†). Moreover, device B2 presents an emission peak at 470 nm with a narrow full width at half-maximum (FWHM) of 58 nm, which is

useful for blue emission of OLEDs. As depicted in Fig. 4D, device B1 achieves a maximum forward-viewing EQE of 4.51% and a CE of 5.54 cd A^{-1}. Whereas, B2 gives a maximum EQE of 8.10% and a CE of 10.62 cd A^{-1}. More importantly, the EQE and CE of B2 also remain high at values of 6.97% and 9.09 cd A^{-1} at a luminance of 1000 cd m^{-2}, demonstrating the low efficiency roll-off of the device. Meanwhile, the power efficiency of these devices shows identical results (Fig. S8 and Table S5, ESI†).

Meanwhile, the doped devices were also fabricated with a configuration of ITO/HAT-CN (5 nm)/TAPC (60 nm)/TCTA (5 nm)/EML (20 nm)/TmPyPB (40 nm)/LiF (1 nm)/Al using 2,6-bis(3-(9H-carbazol-9-yl)phenyl)pyridine (26DCZPPy) as the host and TPA-An-mPhCz as the guest with different doping concentrations (device 1:10%, device 2:20%, and device 3:50%). As shown in Table S6 (ESI†), the TPA-An-mPhCz based doped devices show blue emission with EL peaks at 458, 462 and 474 nm at low operation voltages, respectively (Fig. S9A and B, ESI†). Among the fabricated doped OLEDs, device 3 achieves a maximum EQE of 5.60%, a CE of 7.82% and a PE of 5.85%. These EL spectra remain stable when the voltage increased from 4 to 7 V, confirming their good color stability (Fig. S10, ESI†). However, these values are far behind those of device B2 (Fig. S9C, D and S11, ESI†), suggesting the advantages of non-doped OLEDs using AIEgens as EMLs.

It is worth noting that the EQE of device B2 breaks through the theoretical limit (5%) of pure fluorescent OLEDs. Theoretically, the EQE equals $\eta_{eh} \times \eta_{PL} \times \eta_{exciton} \times \eta_{out}$, where η_{eh} is the factor of the recombination efficiency of injected holes and electrons (ideally 100%), η_{PL} is the absolute Φ_F of the emitter (65.1% for the vacuum evaporated films of TPA-An-mPhCz), $\eta_{exciton}$ is the radiative exciton ratio, and η_{out} is the light out-coupling efficiency. We measured the angle-dependent PL of TPA-An-mPhCz, but no data were obtained. Therefore, η_{out} is assumed to be 20%. According to the above equation, the $\eta_{exciton}$ value of the non-doped OLED is calculated to be 62.2% using TPA-An-mPhCz as the EML, which is suggestive of the involvement of triplet excitons in the radiative process.

To verify the improved mechanism in the EL efficiency of the TPB–An–mPhCz-based OLED, we first measured the fluorescence lifetime of the TPA-An-mPhCz film, which shows a single-exponential decay process with the value of 3.58 ns. Then, we obtained its T_1 energy level by measuring its phosphorescent spectrum according to a reported method,[20] which is deduced to be 1.76 eV (Fig. S12, ESI†). These results suggest that TPA-An-mPhCz possesses a large energy gap between S_1 and T_1. Therefore, TADF was excluded from the high performance OLED.

Next, the transient EL decay of the non-doped device at different voltages was analyzed. As shown in Fig. 5A, the EL decay exhibits two parts, the prompt fluorescence and the delayed fluorescence. Triplet excitons return directly to higher excited singlet states, which results in no delayed component in the transient EL spectra of the hybridized local and charge transfer (HLCT)-OLEDs.[23] Thus, the emission mechanism should be TTU. The prompt part originates from singlet exciton emission under electrical pumping, and the following delayed component is attributed to triplet excitons *via* the TF process.

Fig. 4 (A) Device structure and ionization potentials (IPCV) and electron affinities (EACV) for each material. (B) Current density–voltage–luminance (*J*–*V*–*L*) characteristics of devices B1 and B2. (C) Electroluminescence (EL) spectra of device B2 at various voltages. (D) CE and EQE *versus* luminance curves of the non-doped OLEDs based on the AIEgens TPA-An-Ph and TPA-An-mPhCz.
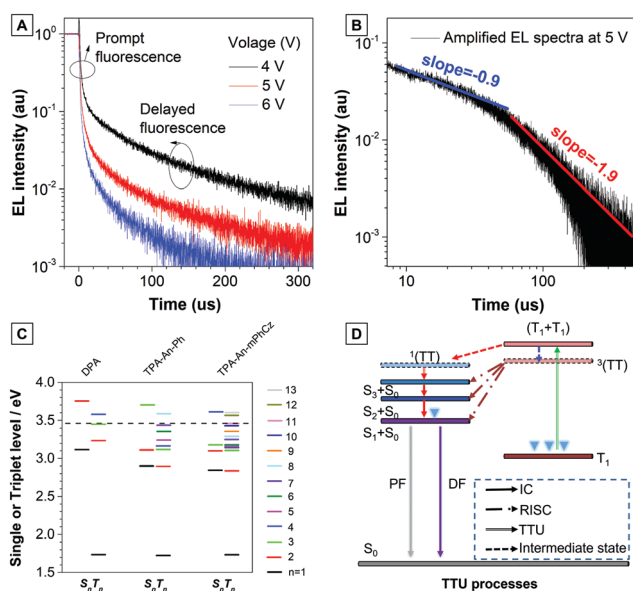

Fig. 5 (A) Transient EL decay of the non-doped device B2 at different voltages. (B) Amplified EL spectra of the non-doped device B2 at 5 V. (C) Energy diagrams. Energy levels and twice the T_1 energies (dashed line) of the anthracene derivatives calculated using B3LYP/6-311G(d,p), where *n* is the quantum number used to indicate the excited state. (D) Proposed TTU mechanism based on the emitters.

Moreover, the ratio of delayed fluorescence slowly decreases with increasing voltage. It is hypothesized that the delayed portion is not simply from the recombination of the trapped charges.[11b] As reported by Kondakov *et al.*, the delayed EL is proportional to t^{-2} (*t* is the time) when TTU is predominant in the OLED.[25] The plot of log(EL intensity) *versus* log(*t*) for device

B2 is shown in Fig. 5B. The slope of the obtained curve is nearly −2, which is consistent with the TTU-related triplet exciton dynamics described above, further confirming the existence of a TTU process in the TPA-An-mPhCz-based OLED.

To further confirm our assumptions, the excited states of DPA, TPA-An-Ph, and TPA-An-mPhCz were calculated using TD-DFT calculations based on the B3LYP/6-311(d,p) basis set. As shown in Fig. 5C, the T_1 energy levels of DPA, TPA-An-Ph and TPA-An-mPhCz are all close to 1.73 eV, which is consistent with the results reported in the literature that were derived from the ^{3}LE state of an anthracene unit.[26] Thus, their ^{3}(TT) are almost identical. In addition, the energy of $2T_1$ is higher than that of T_2, indicating that η_{TTU} is close to 20% and in turn leading to an $\eta_{exciton}$ value of 32.5%. However, the scenario cannot explain the maximum EQE of the TPA-An-mPhCz based OLED. Therefore, the possibility of a conversion process from ^{3}(TT) to S_n (≤ 3) should be considered. According to previous work,[12] the spin–orbit interaction between S_n and T_m whose energy levels are close to that of ^{3}(TT) and in the range of 3.40–3.50 eV (Table S7, ESI†), should be taken into account. The TTU transition would form S_n and then return to S_1 *via* internal conversion. The possible TTU transitions from ^{3}(TT) to S_n are given in Table S8 (ESI†). For TPA-An-Ph (Fig. S13, ESI†) and TPA-An-mPhCz (Fig. S14, ESI†), the TTU transition involves different vectors of the magnetic moments. For example, as depicted in Fig. S14 and Table S8 (ESI†), the spin–orbit matrix of $\langle S_3|H_{so}|T_{10}\rangle$ consisting of HOMO−2 and HOMO−4 are involved in the TTU transition from ^{3}(TT) to S_n for TPA-An-mPhCz. The HOMO−4 is localized on the anthracene unit, whereas HOMO−2 is mainly localized on the carbazole unit, which is oriented perpendicularly to the anthracene unit. As a

result, the rotation of the molecular orbitals from the carbazole unit to the anthracene unit is involved in the spin–orbit matrices, leading to a TTU process according to spin conversion, as illustrated in Fig. 5D. This process is different from HLCT and the "Hot" exciton process because the observed delayed fluorescence in OLEDs is derived from the TTU process.

Conclusions

Novel blue AIEgens of TPA-An-Ph and TPA-An-mPhCZ were designed and synthesized. They show excellent thermal stability and high Φ_F in their film states. The non-doped OLEDs exhibit excellent device performance. The maximum CE and EQE of the TPA-An-mPhCz-based OLED can reach up to 10.62 cd A^{-1} and 8.10%, respectively, with an operation voltage as low as 3.0 V. More importantly, the CE and EQE still remain high at values of 9.09 cd A^{-1} and 6.97%, respectively, at a luminance of 1000 cd m^{-2}, which is suggestive of a low efficiency roll-off of the device. The transient EL spectrum and theoretical calculations confirm that the unique TTU process of the emitter plays a crucial role in achieving the high EQE. The design strategy of a combination of the TTU process and AIE effect is valuable for the construction of high-performance OLEDs, which might be beneficial for practical applications, such as white lighting and full color, flat-panel displays.

Author contributions

P. Han, A. Qin and B. Z. Tang conceived the original idea for investigation. P. Han, K. Wang, A. Qin and B. Z. Tang wrote the manuscript. P. Han synthesized the compounds. P. Han, and Y. Qiu measured the photophysical, thermal and electrochemical properties of the compounds. C. Lin and D. Ma fabricated and characterized the devices. P. Han performed the X-ray single crystal diffraction analysis. P. Han and H. Wu performed the quantum chemical calculations. All authors discussed the progress of research and reviewed the manuscript.

Conflicts of interest

There are no conflicts to declare.

Acknowledgements

References

1 (a) C. W. Tang and S. A. VanSlyke, *Appl. Phys. Lett.*, 1987, **51**, 913–915; (b) J. Kido, M. Kimura and K. Nagai, *Science*, 1995, **267**, 1332–1334; (c) Y. Sun, N. C. Giebink, H. Kanno, B. Ma, M. E. Thompson and S. R. Forrest, *Nature*, 2006, **440**, 908–912.

2 W. Helfrich and W. G. Schneider, *J. Chem. Phys.*, 1966, **44**, 2902–2909.

3 (a) H. Kuo, Y. Chen, L. R. Devereux, C. Wu, M. A. Fox, C. Kuei, Y. Chi and G. Lee, *Adv. Mater.*, 2017, **29**, 1702464; (b) C. Adachi, M. A. Baldo, M. E. Thompson and S. R. Forrest, *J. Appl. Phys.*, 2001, **90**, 5048–5051.

4 A. Endo, M. Ogasawara, A. Takahashi, D. Yokoyama, Y. Kato and C. Adachi, *Adv. Mater.*, 2009, **21**, 4802–4806.

5 H. Uoyama, K. Goushi, K. Shizu, H. Nomura and C. Adachi, *Nature*, 2012, **492**, 234–238.

6 (a) J. U. Kim, I. S. Park, C. Chan, M. Tanaka, Y. Tsuchiya, H. Nakanotani and C. Adachi, *Nat. Commun.*, 2020, **11**, 1–8; (b) K. Tuong, Ly, R. Chen-Cheng, H. Lin, Y. Shiau, S. Liu, P. Chou, C. Tsao, Y. Huang and Y. Chi, *Nat. Photonics*, 2017, **11**, 63–68; (c) J. Lee, C. Chen, P. Lee, H. Lin, M. Leung, T. Chiu and C. Lin, *J. Mater. Chem. C*, 2019, **7**, 5874–5888.

7 (a) C. Ganzorig and M. Fujihira, *Appl. Phys. Lett.*, 2002, **81**, 3137–3139; (b) D. Y. Kondakov, T. D. Pawlik, T. K. Hatwar and J. P. Spindler, *J. Appl. Phys.*, 2009, **106**, 124510.

8 (a) A. Salehi, C. Dong, D. Shin, L. Zhu, C. Papa, A. Thy Bui, F. N. Castellano and F. So, *Nat. Commun.*, 2019, **10**, 1–9; (b) J. Huh, Y. H. Ha, S. Kwon, Y. Kim and J. Kim, *ACS Appl. Mater. Interfaces*, 2020, **12**, 15422–15429; (c) X. Qiao and D. Ma, *Mater. Sci. Eng., R*, 2020, **139**, 100519.

9 (a) C. Chiang, A. Kimyonok, M. K. Etherington, G. C. Griffiths, V. Jankus, F. Turksoy and A. P. Monkman, *Adv. Funct. Mater.*, 2013, **23**, 739–746; (b) T. L. Keevers and D. R. McCamey, *Phys. Rev. B*, 2016, **93**, 045210; (c) B. H. Wallikewitz, D. Kabra, S. Gélinas and R. H. Friend, *Phys. Rev. B: Condens. Matter Mater. Phys.*, 2012, **85**, 045209.

10 Y. Y. Cheng, T. Khoury, R. G. C. R. Clady, M. J. Y. Tayebjee, N. J. Ekins-Daukes, M. J. Crossley and T. W. Schmidt, *Phys. Chem. Chem. Phys.*, 2010, **12**, 66–71.

11 (a) D. Di, L. Yang, J. M. Richter, L. Meraldi, R. M. Altamimi, A. Y. Alyamani, D. Credgington, K. P. Musselman, J. L. MacManus-Driscoll and R. H. Friend, *Adv. Mater.*, 2017, **29**, 1605987; (b) W. Liu, S. Ying, R. Guo, X. Qiao, P. Leng, Q. Zhang, Y. Wang, D. Ma and L. Wang, *J. Mater. Chem. C*, 2019, **7**, 1014–1021.

12 R. Ieuji, K. Goushi and C. Adachi, *Nat. Commun.*, 2019, **10**, 5283.

13 R. Sato, H. Kitoh-Nishioka, K. Kamada, T. Mizokuro, K. Kobayashi and Y. Shigeta, *J. Phys. Chem. C*, 2018, **122**, 5334–5340.

14 J. Yang, Z. Chi, W. Zhu, B. Z. Tang and Z. Li, *Sci. China Chem.*, 2019, **62**, 1090–1098.

15 (a) Z. Zhao, H. Zhang, J. W. Y. Lam and B. Z. Tang, *Angew. Chem., Int. Ed.*, 2020, **59**, 2–22; (b) J. Yang, M. Fang and Z. Li, *Aggregate*, 2020, **1**, 6–18.

16 J. Mei, N. L. C. Leung, R. T. K. Kwok, J. W. Y. Lam and B. Z. Tang, *Chem. Rev.*, 2015, **115**, 11718–11940.

17 S. Sasaki, S. Suzuki, W. M. C. Sameera, K. Igawa, K. Morokuma and G. Konishi, *J. Am. Chem. Soc.*, 2016, **138**, 8194–8206.

18 P. Han, C. Lin, D. Ma, A. Qin and B. Z. Tang, *ACS Appl. Mater. Interfaces*, 2020, **12**, 46366–46372.

19 H. Liu, D. Cong, B. Li, L. Ye, Y. Ge, X. Tang, Y. Shen, Y. Wen, J. Wang, C. Zhou and B. Yang, *Cryst. Growth Des.*, 2017, **17**, 2945–2949.

20 X. Tang, Q. Bai, T. Shan, J. Li, Y. Gao, F. Liu, H. Liu, Q. Peng, B. Yang, F. Li and P. Lu, *Adv. Funct. Mater.*, 2018, **28**, 1705813.

21 R. Hu, E. Lager, A. Aguilar-Aguilar, J. Liu, J. W. Y. Lam, H. H. Y. Sung, I. D. Williams, Y. Zhong, K. S. Wong, E. Peña-Cabrera and B. Z. Tang, *J. Phys. Chem. C*, 2009, **113**, 15845–15853.

22 H. Nie, K. Hu, Y. Cai, Q. Peng, Z. Zhao, R. Hu, J. Chen, S. Su, A. Qin and B. Z. Tang, *Mater. Chem. Front.*, 2017, **1**, 1125–1129.

23 W. Li, Y. Pan, L. Yao, H. Liu, S. Zhang, C. Wang, F. Shen, P. Lu, B. Yang and Y. Ma, *Adv. Opt. Mater.*, 2014, **2**, 892–901.

24 J. Guo, X. Li, H. Nie, W. Luo, S. Gan, S. Hu, R. Hu, A. Qin, Z. Zhao, S. Su and B. Z. Tang, *Adv. Funct. Mater.*, 2017, **27**, 1606458.

25 D. Y. Kondakov, *J. Appl. Phys.*, 2007, **102**, 114504.

26 S. Reineke and M. A. Baldo, *Sci. Rep.*, 2014, **4**, 3797.